![AGU ADVANCING EARTH AND SPACE SCIENCE]

Water Resources Research®

Key Points:

- We propose a novel method to determine the groundwater flow rate using the actively heated fiber optics based thermal response test
- The method minimizes the effect of borehole grout by separating its contribution to the heat transfer
- A validation at a bank collapse site is provided and the groundwater flow rate distribution along the borehole is obtained

Supporting Information:

Supporting Information may be found in the online version of this article.

Correspondence to:

K. Gu,
gukai@nju.edu.cn

Author Contributions:

Conceptualization: Bo Zhang, Kai Gu, Baojun Wang
Data curation: Haibo Qi
Formal analysis: Bo Zhang, Peter Bayer
Funding acquisition: Kai Gu, Peter Bayer, Bin Shi
Investigation: Bo Zhang, Haibo Qi, Yuehua Jiang, Quanping Zhou
Methodology: Bo Zhang, Kai Gu, Haibo Qi
Project Administration: Kai Gu, Bin Shi, Yuehua Jiang, Quanping Zhou
Resources: Yuehua Jiang, Quanping Zhou
Software: Bo Zhang
Supervision: Kai Gu, Baojun Wang
Validation: Bo Zhang, Peter Bayer, Haibo Qi
Writing – original draft: Bo Zhang
Writing – review & editing: Kai Gu, Peter Bayer

Estimation of Groundwater Flow Rate by an Actively Heated Fiber Optics Based Thermal Response Test in a Grouted Borehole

Bo Zhang[1] ![ID], **Kai Gu[1,2]** ![ID], **Peter Bayer[3]** ![ID], **Haibo Qi[1]**, **Bin Shi[1]** ![ID], **Baojun Wang[1]**, **Yuehua Jiang[4]**, and **Quanping Zhou[4]**

[1]School of Earth Sciences and Engineering, Nanjing University, Nanjing, China, [2]Frontiers Science Center for Critical Earth Material Cycling, Nanjing University, Nanjing, China, [3]Institute of Geosciences and Geography, Martin Luther University Halle-Wittenberg, Halle, Germany, [4]Nanjing Center, China Geological Survey, Nanjing, China

Abstract The thermal response test (TRT) in an aquifer establishes a relationship between the groundwater flow rate and the recorded temperature response curve of temporal ground heating. A major challenge for achieving a mature hydrogeological field test is to minimize borehole effects by smart practical solutions of in situ heating and temperature sensing. When borehole effects are substantial, concepts are needed to separate their contribution to the recorded signal. This is especially the case when heating and sensing devices are installed in grouted boreholes as permanent testing stations. Interpretation of a recorded response curve thus means solving a transient heat transfer problem with radial conduction through composite media. Here, a series of numerical models are set up to study the effect of the grout and the jacket of an actively heated fiber-optic cable on the simulated thermal response measured along a heated borehole. The findings are utilized to further develop existing groundwater flow rate estimation procedures based on the moving infinite line source model. The developed approach is demonstrated in a case study in a borehole near a bank collapse site that penetrates different aquifer layers. Accordingly, significant local groundwater flow rates (9×10^{-7}–5×10^{-6} m·s^{-1}) are found that vary with depth. The values derived by the TRT interpretation closely match the expected rates (2×10^{-6}–7×10^{-6} m·s^{-1}), which supports the good applicability of the estimation procedure in the field.

1. Introduction

Proper knowledge of the groundwater flow rate is vital to water resource management, contaminant control, hydraulic structure design, and shallow geothermal energy exploitation (Bense et al., 2016; Herrera-García et al., 2021; Stauffer et al., 2019; Xue et al., 1990). Due to the diversity of hydraulic conditions and the often-significant heterogeneity of aquifers, reliable estimation is only feasible by field investigation (Brunner et al., 2017; Hermans et al., 2022; Ye et al., 2004). Most commonly, flow meters or tracer tests are applied for direct measurement, or piezometers are used to determine the direction and rate of groundwater flow. These methods are difficult to obtain refined results from the perspective of the economy. Due to their low cost and environmentally friendly nature, thermal tracing methods have been widely used in recent years (Anderson, 2005; Hoffmann et al., 2021; Selker et al., 2006). The underlying principle is measuring the effect of advection on the thermal regime in the subsurface, which can be used to quantify local groundwater flow rates and also their variability at a larger scale. For this, either passive temperature measurements that monitor the natural thermal fluctuations are employed (Kurylyk & Irvine, 2016; Molina-Giraldo, Bayer, Blum, Cirpka, 2011), or heat is actively induced into the aquifer (Q. Liu et al., 2022; Sarris et al., 2018; Wagner, Li, et al., 2014). Active heating of groundwater is more demanding but advantageous, since controlled thermal modifications and high thermal gradients can be achieved. This enables the identification of the variable role of convection more accurately and even at a small scale, which is otherwise blurred by omnipresent heat diffusion.

An active method established in the area of shallow geothermal energy evolution for investigating the effective thermal conductivity around borehole heat exchangers is the thermal response test (TRT) (Spitler & Gehlin, 2015), which is based on the infinite line source (ILS) theory. To obtain the refined thermal conductivity of the strata within a short test time, previous studies have focused on modified borehole radius or grouting, on alternative heating techniques (e.g., heating cable), and special methods of measuring the temperature evolution in-situ (wireless sensor, distributed temperature sensing) (Acuña & Palm, 2013; Bayer et al., 2016; Cao et al., 2019; Freifeld et al., 2008; Hakala et al., 2021; Raymond et al., 2015; Wagner et al., 2012; Wilke et al., 2020; C. Zhang

et al., 2014; Zhao et al., 2020). In particular, the actively heated fiber optics based thermal response test (ATRT) can resolve the heterogeneous thermal conductivity of the strata around the borehole within a reasonable amount of time (He et al., 2018; B. Zhang et al., 2020). Here, an actively heated fiber-optic cable (AHFOC) is applied in the tube, open borehole, or grout, and the vertical variation of effective thermal conductivity is derived by inverting the recorded depth-dependent temperature response curves with the ILS. With the use of AHFOC, ATRT provides a suitable TRT method and can satisfy the ILS theory. Current research has solved the ground thermal conductivity estimation problem when only considering heat conduction based on ILS theory. On the other hand, for estimating the groundwater flow rate from TRTs, the moving infinite line source (MILS) theory has been suggested instead (Angelotti et al., 2018; Van de Ven et al., 2021; Verdoya et al., 2018; Wagner, Bayer, et al., 2014; Wagner et al., 2013). MILS theory was proposed by Sutton et al. (2003) and Diao et al. (2004) with a moving heat source assumption. The analytical solution has provided a theoretical basis and practical tool for estimating groundwater flow rate. A MILS model facilitates distinguishing the contribution by thermal conduction and horizontal convection, and this works best when any influence from the borehole installation can be neglected.

The concept of ATRT has become popular for evaluating groundwater flow in porous media and fractures (Bakker et al., 2015; Bense et al., 2016; des Tombe et al., 2019; Munn et al., 2020; Pouladi et al., 2021; Selker & Selker, 2018), as it provides distributed measurements. There are different methods for establishing the relationship between the groundwater flow rate and the temperature response curve of a linear heat source. G. Liu et al. (2013) demonstrated the role of groundwater flow at different depths in a borehole by nonuniform temperature trends during heating. Read et al. (2014) reported that the temperature difference between a heated fiber optic cable and a nonheated reference cable can be related to borehole vertical fluid rates. Bense et al. (2016) discussed TRTs in fractured rock. The results showed that the measured abrupt temperature variation correlated with a change of the groundwater flow rate. Selker and Selker (2018) used the stable temperature rise in the thermal response to estimate groundwater flow rates. des Tombe et al. (2019) designed a 24 mm drive rod with an optical cable for temperature measurement and a heating cable for groundwater flow rate measurement. The drive rod was installed by direct-push in direct contact with surrounding strata to meet the linear heat source assumption (direct contact between heat source and ground), and the MILS was employed to calculate the groundwater flow rate at various depths. Borehole effects such as by grout in borehole heat exchangers hamper the application of the MILS (Van de Ven et al., 2021; Wagner, Bayer, et al., 2014). The applicability of direct-push, however, is limited to unconsolidated sediments and shallow depths.

Some previous studies focused on shallow geothermal energy research illustrated these inconsistent conditions, which do not meet the requirements of a linear heat source, could change the temperature response curve in TRT, and the change weakened with time (Pasquier, 2018; B. Zhang et al., 2020). A TRT usually requires more heating time to estimate a lower error thermal conductivity in a borehole. Considering groundwater flow estimation based on a borehole, how to apply a suitable TRT would be trickier when such inconsistent conditions happen when considering the heat convection in and around a grouted borehole. AHFOC meets the stringent requirements for a linear heat source, and if these requirements are met, the MILS describes the TRT considering uniform convection in the surrounding aquifer. Since the jacket of AHFOC has low thermal conductivity, the temperature response curve of a TRT cannot be perfectly described by the MILS (Figure S1 in Supporting Information S1, presence of low thermal conductivity). del Val et al. (2021) and Simon et al. (2021) emphasize that the "skin effect" (thermal resistance) caused by the jacket cannot be ignored when estimating the groundwater flow rate. Different stages of thermal response were identified based on heat transfer in the jacket and porous media (subdividing two stages dominated by conduction and convection). Using the MILS, flow rates in porous media can be obtained by calculating so-called inflection feature points of different thermal response stages independent of the jacket effect (Simon et al., 2021). This method was applied in scenarios where the fiber-optic cable is in direct contact with the porous media, such as for vertical flow rate estimation in a riverbed (Simon et al., 2022). A concern similar to the "skin effect" happen in the measurement based on a borehole; the borehole with different thermal conductivity materials would further change the observed temperature response curve. For example, the roles of water filling in the borehole or grouting also need to be considered (Figure S1 in Supporting Information S1). More recently, a greater focus has also been placed on Ground-Borehole-Cable interaction in C. C. Zhang et al. (2020) about distributed strain sensing of the subsurface. How to extract the value of ground properties with borehole effects plays a pivotal role in the measurements.
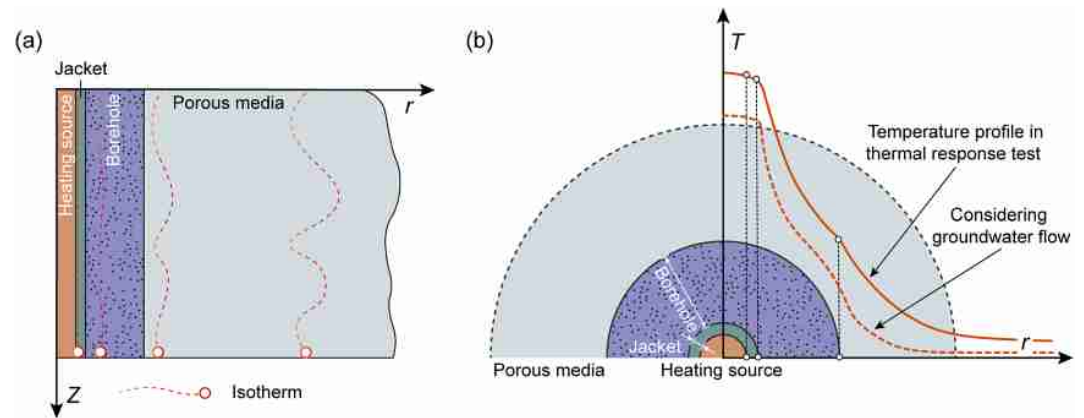
Figure 1. Schematic diagram of the temperature distribution occurring in concentric composite media during the thermal response test. (a) Vertical cross-section of radial temperature distribution with isotherms represented by dashed lines. (b) Top view with characteristic cross-sectional temperature (T) trend with and without groundwater flow.

The applicability of the MILS to such conditions is in the focus of this work. The objective of the present study is to determine the groundwater flow rate from a TRT with AHFOC in a permanent installation considering borehole effects with grout. This article is organized as follows: First, a numerical model of the radial material layers in the borehole is set up to simulate the heat source, jacket, borehole, and porous media heat transfer under different groundwater flow conditions. Then, based on the MILS model, a method for inferring depth-dependent groundwater flow rates is developed. Finally, this method is validated by an ATRT conducted in the field at a bank collapse site with loose sediments.

2. Methodology

2.1. Heat Transfer Processes in and Around a Borehole

Interpreting the TRT using AHFOC can be conceptualized as a transient heat transfer problem in concentric composite media (Figure 1), refering to the setup proposed by B. Zhang et al. (2020). The heat transfer difference is determined by varying the porous media (Figure 1a), and the heat in the vertical direction of the heat source controlled by multilayer media (Figure 1b). The central cable in the grouted borehole generates heat that continuously diffuses outward, driven by the radial temperature gradient. Accordingly, heat accumulates in and around the borehole, decreasing gradually with radial distance (Figure 1b). The temperature gradient is not linear but reflects the different thermophysical properties of the jacket, borehole (filling), and porous media of the ambient ground. If groundwater flow is present, this may accelerate heat dissipation in the ground, and this mitigates the observed temperature rise in the borehole. The combined influence of the thermal material properties and groundwater flow in different layers can be visualized by measuring the heat source temperature evolution as depth-dependent response curves.

In saturated porous media, heat is transported by conduction and convection, whereas convection by groundwater is also termed as a form of advection. For a heterogeneous medium, heat transport in three dimensions (3D) can be described by the corresponding transient advection-dispersion equation (Stauffer et al., 2019):

$$\frac{\partial T}{\partial t} = \nabla(\mathbf{D}\nabla T) - \frac{\rho_w c_w}{\rho c}\nabla(\mathbf{q}T) + \frac{P}{\rho c} \tag{1}$$

where T (K) is the temperature, and t is the time (s). The parameters ρc and $\rho_w c_w$ (J·m^{-3} K^{-1}) are the volumetric heat capacities of the bulk medium and water, respectively, which are assumed to be constant; P (W·m^{-3}) represents the volumetric heat generation in the source term. Considering the relatively small local temperature gradients induced by the in-situ heating, density and viscosity effects can be ignored. For the description of conditions in heterogeneous media, $\mathbf{q}$ (m·s^{-1}) represents the specific water flux vector (Darcy flux), and the thermal dispersion tensor $\mathbf{D}$ (m^2·s^{-1}) denotes spatially variable hydrodynamic dispersion. As heat diffusion dominates, any contribution from mechanical dispersion is commonly assumed to be negligible, and $\mathbf{D}$ thus represents the (effective) thermal diffusivity tensor.

For a long vertical borehole, axial effects may be ignored and vertical heat flow is subordinate to the horizontal flow. Assuming that the groundwater flow is in x-direction within the x-y plane perpendicular to the borehole, heat transport for simplified homogeneous media can be described by (Simon et al., 2021; Stauffer et al., 2019):

$$\frac{\partial T}{\partial t} = D\left(\frac{\partial^2 T}{\partial x^2} + \frac{\partial^2 T}{\partial y^2}\right) - v_{\text{th}}\frac{\partial T}{\partial x} + \frac{P}{\rho c} \tag{2}$$

where the averaged thermal diffusivity D (m^2·s^{-1}) is the ratio between bulk thermal conductivity λ (W·m^{-1} K^{-1}) and volumetric heat capacity ρc (J·m^{-3} K^{-1}):

$$D = \frac{\lambda}{\rho c} \tag{3}$$

and the velocity v_{th} (m·s^{-1}) of a thermal front in homogeneous porous media with Darcy flux q (m·s^{-1}) is:

$$v_{\text{th}} = \frac{\rho_{\text{w}} c_{\text{w}}}{\rho c} q \tag{4}$$

The Darcy flux, q, is the specific discharge or groundwater flow rate, and can be used to compute the groundwater flow velocity, v, for a given effective porosity. In comparison, a temperature signal travels at retarded velocity, v_{th}. For a given total porosity n (%), which equals the volumetric water content for saturated conditions, the bulk-specific heat capacity is the weighted arithmetic mean of the specific heat capacity of water, $\rho_{\text{w}} c_{\text{w}}$, and solid, $\rho_s c_s$:

$$\rho c = n\rho_{\text{w}} c_{\text{w}} + (1-n)\rho_s c_s \tag{5}$$

2.2. MILS Model

The MILS can be used for separating the contributions from conduction and convection to the thermal response (Wagner et al., 2013). The assumptions of ideal conditions include (a) ideal borehole conditions in which the linear heat source is in direct contact with the porous media with no additional thermal resistance, (b) the porous media is uniform and infinite, (c) the flow rate of the fluid is uniform and stable in the porous media, and (d) any temperature-dependent changes in the thermal properties of the groundwater can be ignored (des Tombe et al., 2019; Diao et al., 2004; Molina-Giraldo, Bayer, Blum, 2011; Molina-Giraldo, Blum, et al., 2011). For constant input of heat per length unit of the borehole, p (W·m^{-1}), the transient relative temperature change (K) of the linear heat source ([x,y] $\to$ [0,0]) can be expressed as (des Tombe et al., 2019):

$$\Delta T = \frac{p}{4\pi\rho c D}\exp\left(\frac{r}{B}\right)W\left(\frac{A}{t}, \frac{r}{B}\right) \tag{6}$$

$$A = \frac{r^2}{4D} \tag{7}$$

$$B = 2D\frac{\rho c}{q\rho_{\text{w}} c_{\text{w}}} \tag{8}$$

$$W\left(\frac{A}{t}, \frac{r}{B}\right) = \int\limits_{A/t}^{\infty}\frac{1}{S}\exp\left(-s - \frac{r^2}{4B^2 s}\right)ds \tag{9}$$

where $\Delta T = T - T_0$; T_0 (K) is the undisturbed temperature, p (W·m^{-1}) is the specific heating power of the heating source, r (m) is radius of the heating source, and W is equivalent to the Hantush well function (Hantush, 1956). The modified Bessel function of the second kind and order zero is represented by K_0. The corresponding steady-state temperature representing an upper limit, $\Delta T(t_\infty)$, can expressed as (des Tombe et al., 2019):

$$\Delta T(t_\infty) = \frac{p}{2\pi\rho c D}\exp\left(\frac{r}{B}\right)K_0\left(\frac{r}{B}\right) \tag{10}$$

$\Delta T(t_\infty)$ is approximately reached after sufficiently long heating during a TRT. This is only related to the thermal conductivity and groundwater flow rate in the aquifer. The temperature rise of the line heat source can be expressed by relating to $\Delta T(t_\infty)$ as:

$$\Delta T = \frac{\Delta T(t_\infty)}{2K_0\left(\frac{r}{B}\right)}W\left(\frac{A}{t}, \frac{r}{B}\right) \tag{11}$$

Reaching $\Delta T(t_\infty)$ will take longer, the lower the role of convection is. In case of no groundwater flow, the temperature increases continuously with time. Then, the temperature rise of the line heat source is:

$$\Delta T = \frac{p}{4\pi\rho c D}W\left(\frac{r^2}{4Dt}\right) \tag{12}$$

When the heat source radius r is sufficiently small, and the heating time t is sufficiently long, that is, $r^2/4Dt \leq 0.01$ (Yeh et al., 2015), Equation 11 can be simplified as (the ILS model):

$$\Delta T = \frac{p}{4\pi\lambda}\ln t + \frac{p}{4\pi\lambda}\ln\left(\frac{2.25D}{r^2}\right) \tag{13}$$

des Tombe et al. (2019) demonstrated that the combination of parameters ($\Delta T(t_\infty)$, A, r/B) converges to a unique value if fitting the temperature response curve of a TRT to Equation 11. The groundwater flow rate can be calculated by des Tombe et al. (2019):

$$q = \frac{1}{\rho_w c_w}\left(\frac{r/B}{\sqrt{A}}\sqrt{\lambda\rho c}\right) \tag{14}$$

For non-ideal conditions, Simon et al. (2021) suggested to define feature time points along the thermal response to distinguish the effect of the jacket around the heating cable. Time t_s is the required time to reach steady state if $\Delta T = 0.99\Delta T(t_\infty)$, as suggested by Diao et al. (2004), t_i differentiates the conduction-dominant stage and convection-dominant stage by combining Equations 7 and 13, t_d is the point in time where groundwater flow begins to affect the thermal response considering the effect of the jacket, and at time t_c the effect of the cable jacket becomes negligible. The values of t_s, t_i, and t_d depend on the value of q, which may be expressed as (Simon et al., 2021):

$$q \approx \sqrt{\frac{\lambda}{2\rho c t_d}} \approx \sqrt{\frac{2.24\lambda}{t_i}\frac{\rho c}{\rho_w^2 c_w^2}} \approx \sqrt{\frac{4\lambda}{t_s}\frac{\rho c}{\rho_w^2 c_w^2}} \tag{15}$$

where a graphical method is helpful to identify these feature points. A mean error of the estimated groundwater flow rate of around 4.7% was reported when AHFOC was in direct contact with the ambient ground (Simon et al., 2021). In practice, referring to t_s for estimation of q is most time-consuming as it represents the time of the experiment to reach steady state.

For resolving groundwater flow rates in different depths, the response is commonly examined for discretized sections of the borehole. For instance, every meter of the borehole, Equations 14 or 15 are employed to the corresponding depth-dependent temperature response curves. The discretization is commonly oriented at the spatial resolution of the DTS device.

The concepts for applying the procedures presented by des Tombe et al. (2019) and Simon et al. (2021) are appealing but less caring for grouted boreholes. Sand, bentonite, or cement grout in a borehole cover a much larger radius than the AHFOC itself (Figure 1, the radius of a typical AHFOC is generally 15–30 times smaller than a borehole) and induce thermal resistance that complicates the detection and quantification of groundwater flow. Developing a theoretical model of ATRT in a grouted borehole is challenging and needs to account for the superpositioning effects of heat source, jacket, grout, and ground (Bergman et al., 2011). The solution to this problem builds up on the concept of the "skin effect" proposed by Simon et al. (2021). Further, different stages of the temperature response curve are distinguished, corresponding to the different media. In contrast, however, there is no referral to fixed feature points (t_s, t_d) that differentiate conduction-dominated from convection-dominated phases. During radial heat propagation, the curve reflects the conditions in the different media in and around the grouted borehole
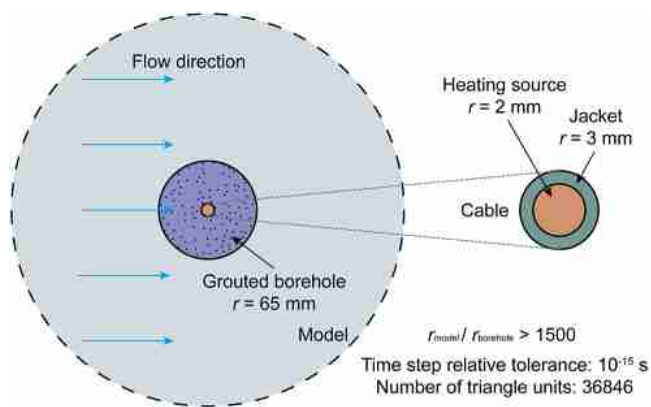
Figure 2. Numerical model geometry: the model simulates heat transfer with convection in composite media using COMSOL Multiphysics®.

in a sequential fashion. During the same process, the heat transfer undergoes the transition from conduction-dominated to convection-dominated phases. Such heat transfer influence factors overlay in time, which hamper the extract the information used to estimate flow rate. For separating these phases, first a numerical analysis is conducted and then the aim is to find the part of the temperature response curve which agrees with the MILS. Such part would be used to fit the parameters of MILS following des Tombe et al. (2019) for estimation of the groundwater flow rate.

2.3. Numerical Model

A homogenous model is not appropriate for considering the effect of the cable jacket on the TRT and accounting for the borehole effects of the TRT. Instead, a two dimensions (2D) finite element model, based on COMSOL Multiphysics®, is set up. The numerical model represents a horizontal cross-section as illustrated in Figure 2, with the AHFOC embedded in a borehole and the surrounding porous media. The model has a radius of 100 m, including the borehole with a radius of 0.065 m and the AHFOC with a radius of 0.003 m. The model is discretized by "extremely fine triangular meshing law" based on model sizes with COMSOL (including 36,846 units with a 1.752×10^{-7} unit-area ratio in the 31,410 m^2 model), that effectively balance model fineness and computational efficiency. The Heat Transfer in Porous Media (ht) interface in COMSOL was used to model heat transfer in porous media with the mixture rule on energies for the finite element method (Nield & Bejan, 2006). The AHFOC is realized as a central heat source (the materials including copper mesh, stainless steel, Kevlar, and PE, as described in B. Zhang et al., 2020) with a high thermal conductivity λ of 60 W·m^{-1} K^{-1} and a low thermal conductivity jacket (LSZH) of $\lambda = 0.42$ W·m^{-1} K^{-1}. With the reference to typical setups of TRT applied in a borehole (Kavanaugh & Rafferty, 2014), the borehole is backfilled with quartz sand with $\lambda = 2.5$ W·m^{-1} K^{-1}. The surrounding ground is fine sand with $\lambda = 1.8$ W·m^{-1} K^{-1}. To consider variable conditions with realistic groundwater flow rates, a range from $q = 5 \times 10^{-5}$ m·s^{-1} to 1×10^{-9} m·s^{-1} is assumed for the aquifer. The model diameter to borehole diameter ratio of more than 1,500 ensures that scenarios with flow rates up to 5×10^{-5} m·s^{-1} can be accurately simulated (with a boundary temperature rise of less than 10^{-6} K). The TRT is performed with a heating power of 20 W·m^{-1} and a heating time of 72 hr, consistent with related applications (del Val et al., 2021; des Tombe et al., 2019).

2.4. Case Study

For testing ATRT interpretation with a grouted borehole, a field test was conducted at a study site in China for groundwater flow rate estimation. This study area is located in the lower section of the Sima bend of the Yangtze River (Figure 3a), where hydrogeological conditions are complex, and bank collapses frequently occur (Yu et al., 2013; Zhu et al., 2018). Additionally, this study area is near a tidally sensitive river section. Seasonal changes in the river levels are evident, covering a span of around 5 m in 2019–2020 (Gu et al., 2021). The hydrostratigraphy of the site consists of a sequence of several aquifers and aquitards, and the aquifers are hydraulically connected to the Yangtze River. The thermal and physical parameters of the strata tested in the lab in this study area are shown in Table 1. The moisture content of the soil was determined using the oven-drying method and averaged over multiple samples within one stratum. The thermal conductivities and volumetric heat capacities were tested using the dual-probe heat pulse and transient plane source methods.

To study the mechanisms of bank collapse and disaster warning (a Ω-shaped bank collapse of approximately 190 m in the direction perpendicular to the river occurred in winter 2017), four boreholes were installed at a depth of 82 m near the site of the bank collapse (Figure 3a). ATRTs were performed in July 2021 in the drilled and backfilled borehole JD1 (diameter of 130 mm) to estimate depth-dependent groundwater flow rates. The water level is maintained at approximately 5 m below the surface, and two confined aquifers (12.8–45.6 m and 48.8–80.0 m) embedded within silty clay layers are penetrated in the depth range of 0–82 m (Figure 3b). The top aquifer with silt and fine sand is characterized by relatively low hydraulic conductivity. Based on stable pumping tests of single-hole incomplete wells, the hydraulic conductivity of an aquifer at the depth range of 12.8–45.6 m is $K = 1.89 \pm 0.15 \times 10^{-5}$ m·s^{-1}, and the groundwater flow rate in the aquifer is roughly in the range between
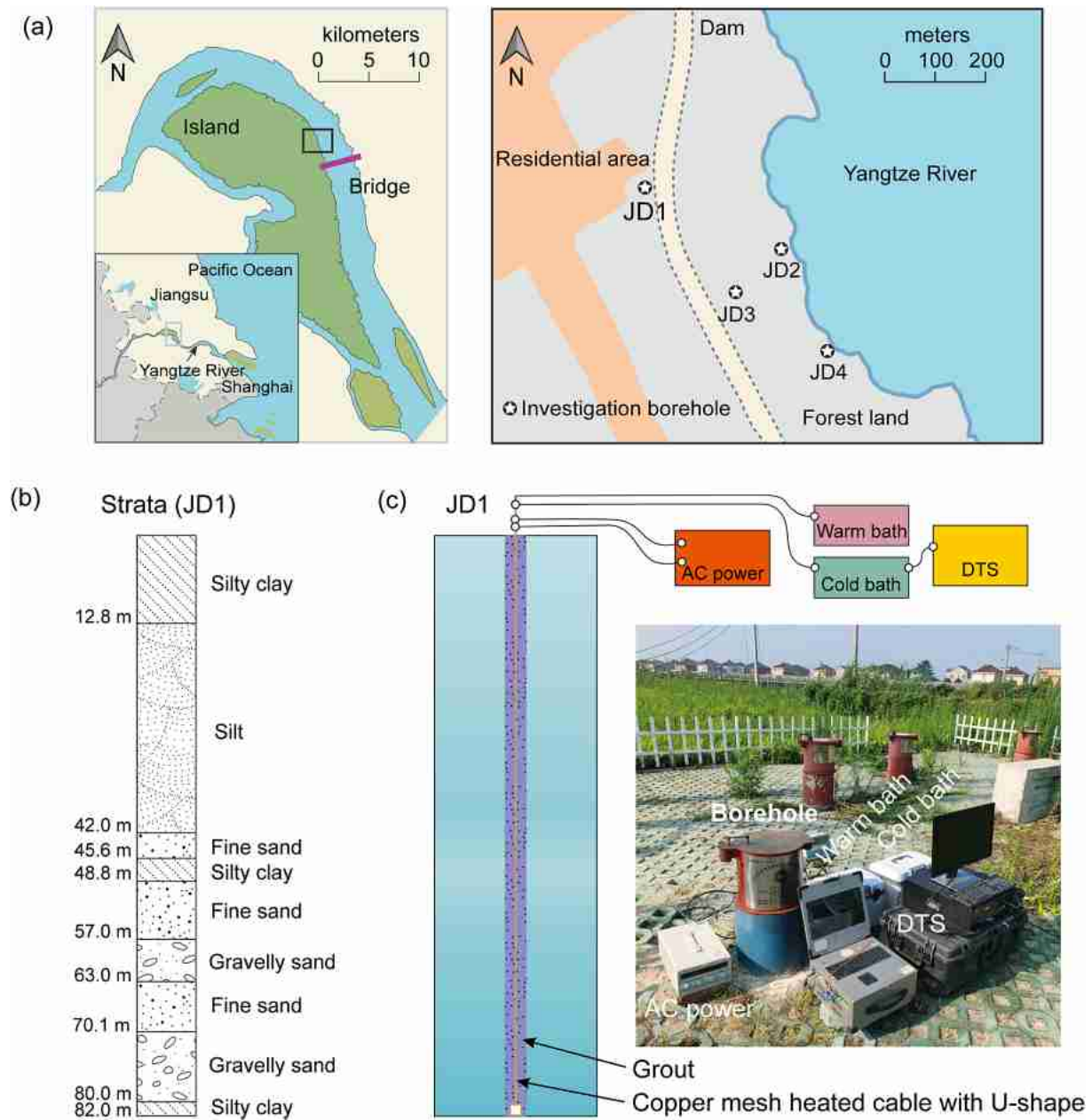
Figure 3. (a) Location map; (b) strata of borehole JD1. (c) Actively heated fiber-optic-based thermal response test (ATRT) field setup.

$q = 9 \times 10^{-7}$ m·s^{-1} and 5×10^{-6} m·s^{-1} considering the changes in the river levels (Gu et al., 2021). Loose sediments such as gravelly sands dominate the bottom, highly permeable aquifer. For the latter, no field tests have been performed and thus no reference values of K and q are available.

Figure 3c illustrates the setup of the ATRT. A copper mesh-heated cable (CMHC, 6 mm diameter, highly integrated) was employed as in-situ heat source and temperature sensor (B. Zhang et al., 2020). Specifically, a U-shaped copper mesh heated fiber-optic cable laid tightly together in the borehole was simplified to serve as a linear heat source (H. Liu et al., 2021). For installation, the CMHC was lowered into the borehole using a metal guide. In order to minimize free convection created by buoyancy forces in the borehole (e.g., Klepikova et al., 2018), it was gradually backfilled with low-permeable quartz sand as the grout ($K_g = 5 \times 10^{-5}$ m·s^{-1}). This was immediately done after lowering the CMHC in the borehole without a casing. This was immediately done after lowering the CMHC in the borehole without a casing. During the lowering and backfilling process, a pulling

Table 1
Physical Media Properties at the Study Area

Strata	Moisture content (%)	Thermal conductivity (W·m^{-1} K^{-1})	Volumetric heat capacity (MJ·m^{-3} K^{-1})
[a] Silty clay	14–34	1.3–1.6	2.1–3.5
[a] Silt	5–24	1.0–1.9	1.5–2.5
[a] Fine sand	6–20	1.2–2.1	1.7–2.8
[a] Gravelly sand	2	1.1	1.4
[b] Quartz sand	Saturated sample	1.8	1.4

[a]Core test (TEMPOS SH-3). [b]Test of grout (HotDisk 2500S).

force equal to the weight of the metal guide was applied to the CMHC by fixing it in the stabilizing bracket on the ground surface. Using the stabilizing bracket, the position of the fiber-optic cable can be carefully controlled and located in the center of the borehole as illustrated in the cross-section in Figure 1. During the ATRT, the CMHC installed in the 0–80 m depth range was uniformly heated for 36 hr at a heating power of 12 W·m^{-1}. The Silixa Ultima-M MK2 DTS device recorded the temperature response of the CMHC every 10 s, with a temperature resolution of 0.01 K and a vertical sampling interval of 0.25 m. By using PT100 probes in both the warm bath and cold bath, we conducted a single-ended calibration, as recommended by Silixa Ltd, to obtain high-quality temperature observations, which are directly used in the paper without any filter, to ensure good data fidelity. The manufacturer specifies an accuracy of 0.1 K for the temperature measurement and a typical spatial resolution of 35 cm.

3. Results
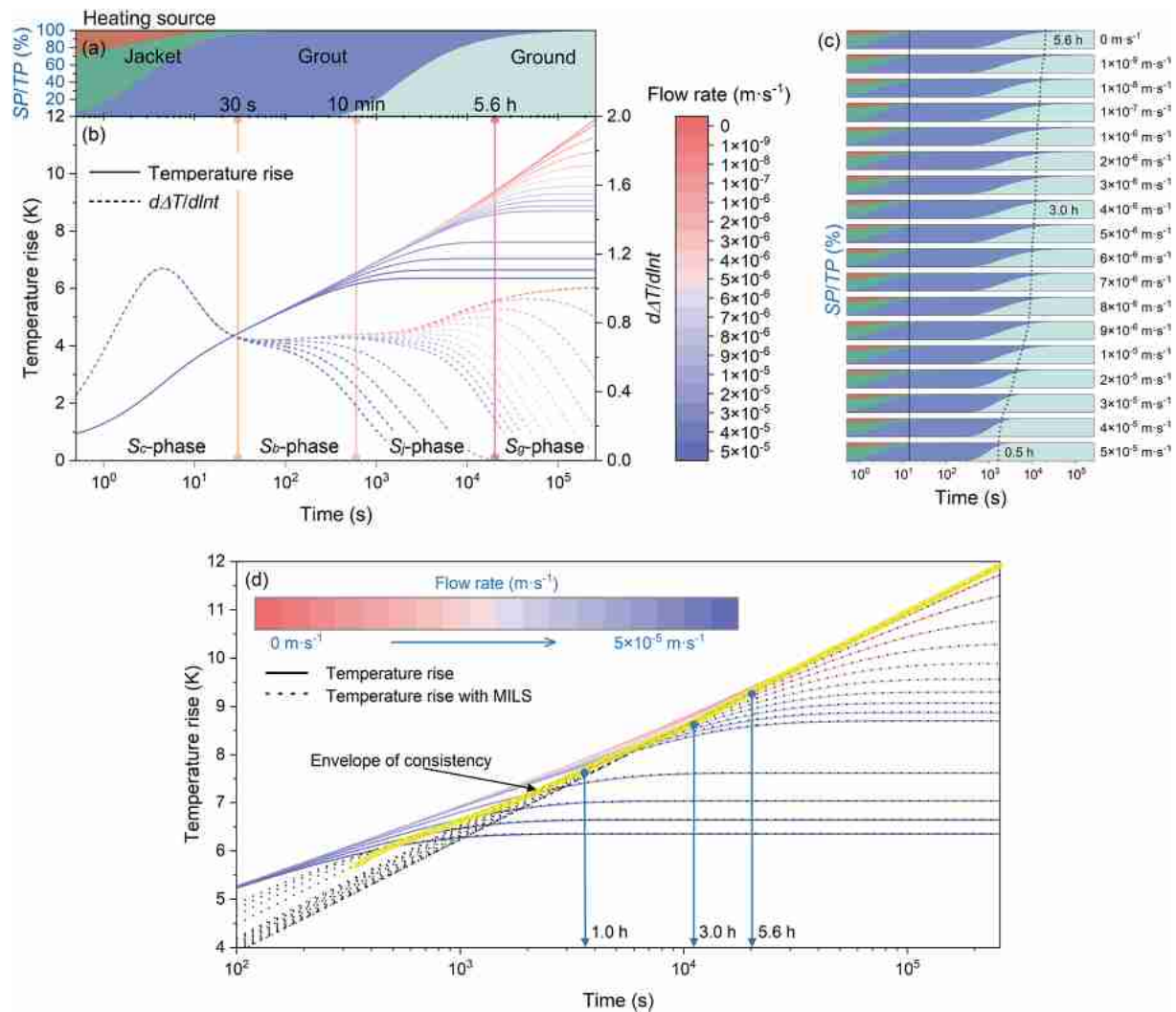
3.1. Numerical Simulation of Thermal Response

Figure 4 shows the simulated temperature response during heating of the composite media in and around the borehole with a central heat source, encircled by a jacket, grout, and ground. The input heat of each media was computed by the corresponding volumetric heat capacity and temperature rise ($E = \rho c \Delta T$); then, the time derivative of the input heat was recorded as the input power of each media (SP = dE/dt). The sum of SP is equal to the total input power (TP), which is the heating power of the ATRT. As the heating power of the ATRT is constant, the change of SP indicates the process of heat transfer in different media. SP/TP = 5% is defined as a threshold (the heat transfer in the medium cannot be ignored) to distinguish different stages of temperature response during heating. The temporal change of SP/TP when the flow rate is zero is shown in Figure 4a. The temperature response curve under different groundwater flow rates is shown in Figure 4b, which also shows the rate of change of temperature rise (temperature response curve) in logarithmic-dΔT/d$ln\,t$. Based on Equation 13, the value of thermal conductivity λ and dΔT/dt have a fixed positive relationship, which only depends on the applied heating power if there is no groundwater flow.

According to the simplified condition $r^2/4Dt \leq 0.01$ for an ideal linear heat source, reaching such a condition is delayed by the thermal resistance of the borehole media. The sequential process of heating of the concentric layers can be delineated by dividing the thermal response into four stages (Figure 4b). If the case with only heat conduction is considered first, these stages are as follows.

- The S_c-phase is the initial stage ($t = 0$–30 s) that is mainly influenced by the material of the AHFOC. During this period, the source and jacket are heating up (SP/TP > 5%), and the effect of both components are illustrated in Figure 4a. However, the heating of the cable is fast, and an effective thermal conductivity obtained by response curve-fitting to a line source solution would reflect the low thermal conductivity of the jacket. This is consistent with the jacket influence period (0–20 s) reported by Simon et al. (2021).
- The S_b-phase covers the period of 0.5–10 min where the borehole dominates the thermal response. The jacket has been heated up, and now the heat front propagates radially through the grout. Accordingly, the effective thermal conductivity characteristic for this phase reflects the high thermal conductivity of the grout. This stage ends when the heating of the ground starts and SP/TP > 5% is reached for this outer medium.
- The S_j-phase is a transitional stage between 10 min and 5.6 hr where borehole and ground properties jointly affect the thermal response curve. This stage is relatively long due to the growing spreading of the thermal front and so the grout is continuously absorbing heat while the ground increasingly affects the effective thermal conductivity that would be derived for this period.
- The S_g-phase starts after $t = 5.6$ hr. Now, the ground plays the dominant role and the heat additionally stored in the grout is negligible (SP/TP < 5%). Fitting the temperature response curve for this period yields a thermal conductivity that is equal to 90% of the true thermal conductivity of the ground, that means the ground thermal conductivity could be efficiently estimated with limited error.

As known from the previous work (del Val et al., 2021; Simon et al., 2021; Wagner et al., 2012), and illustrated in Figures 4a and 4b, temperature response curves become nonlinear on the semi-log scale in the presence of

Figure 4. Thermal response obtained from the actively heated fiber-optic-based thermal response test (ATRT) simulated by the numerical model. (a) Ratio of the input power of each medium (SP) to the total input power (TP) of the ATRT for conditions without groundwater flow. (b) Temperature response curve of the heat source with different groundwater flow rates. The solid line is the temperature, and the dashed line is the derivative of the temperature over time. (c) Ratio of input power of each medium (SP) to total input power (TP) of the thermal response test with different groundwater flow rates. The gray solid line indicates the point when the effect of internally heated fiber-optic cable (S_c-phase) is negligible, and the gray dashed one delineates the onset of the S_g-phase dominated by ambient ground heat transport. (d) Simulated thermal response curves of a grouted borehole media, and theoretical thermal response curves with moving infinite line source (MILS) model for different ambient groundwater flow rates.

groundwater flow. As time increases, the rate of temperature change decreases to zero (dashed line in Figure 4b), and this is accelerated by higher groundwater flow rates. However, the S_c-phase controlled by the AHFOC remains unchanged (Figure 4c). In contrast, the starting point of the S_g-phase is earlier in case of ambient convection. It is 5.6 hr for purely conductive conditions, declines to 3 hr for $q = 4 \times 10^{-6}$ m·s^{-1}, and decreases even further to 0.5 hr for the highest $q = 5 \times 10^{-5}$ m·s^{-1}. This reflects the effect of convection to enhance ambient heat loss. The heat is injected into the ground sooner and faster, and thus, the heat source satisfies the ideal line heat source assumption with respect to the ground earlier. The influence of borehole material decreases as the heating time increases. Due to the steeper lateral thermal gradient by the advective heat loss, their role is mitigated and the onset of the S_g-phase is sooner.

3.2. Estimation of Groundwater Flow Rate

Figure 4d illustrates the comparison of the numerically simulated thermal response curves and the theoretical thermal response curves (MILS theory, Equation 6) for the corresponding groundwater flow rate, q. The

difference between the simulated temperature response curve (colored solid line) and the theoretical temperature response curve (black dotted line) represents the effect of the jacket and grout on the heat transfer. After 5.6 hr of heating, the simulated temperature response curve overlaps with the theoretical temperature influence curve in all scenarios. The overlap phase advances with the groundwater flow rate, reflecting the earlier onset of the S_g-phase as shown in Figure 4d by the yellow envelope. The MILS model thus should be fitted to the responses after the envelope to estimate q, thus mitigating the influence by the additional temperature rise caused by the jacket and borehole.

Unequivocal estimation of q is potentially hampered by the signal-to-noise ratio of the experiment. This is especially relevant for the S_g-stage (Figure 4c), where the temperature changes are small. Obviously, a minor variation in the recorded temperature rise due to measurement errors within the S_g-stage may already be critical for reliable fitting of the MILS. Considering the typical temperature resolution of 0.01 K for most DTS devices, the temperature rise in the S_g-phase is recommended to be no less than 0.5 K. Such degree changes in temperature would guarantee the quality of fit, and reduce the effect of temperature resolution. Based on these considerations, depending on a given q, ideal pre-set time ranges for fitting the response curve are identified.

1. for $t = 1$–72 hr, q can be effectively evaluated in the range of around 1×10^{-5} to 3×10^{-6} m·s^{-1};
2. for $t = 3$–72 hr, q can be estimated within 7×10^{-6} to 2×10^{-6} m·s^{-1};
3. late times of $t = 5.6$–72 hr are especially suitable for $q \leq 10^{-6}$ m·s^{-1}.

In practice, however, q is not given. Therefore, a strategy needs to be defined to exploit the theoretical findings in order to resolve q along the borehole. The following steps are suggested: First, q is estimated simultaneously based on three pre-set time ranges. Next, only those values are kept that are consistent with the valid ranges of q for each phase, and these values represent the groundwater flow rate in ground.

3.3. Results of Field Application

The thermal response over depth and total time of 36 hr for the ATRT performed in July 2021 in the backfilled borehole JD1 (Figure 3) is shown in Figure 5a. Temperature measurements above 5 m reflect partially saturated soils, and they are affected by fluctuations in surface temperatures. Aside from this, the metal guide tends to interfere with temperature measurements in the bottom 2 m of the borehole. Accordingly, these axial portions of the borehole are excluded from the inversion. This highly integrated radially symmetrical structure maintains a constant position relationship between the temperature measuring fiber-optic and the heated resistance of the CMHC. Thus, the temperature rises of the CMHC that vary with depth reflect the changes in the properties of surrounding media but are not compromised by misplacement in the borehole. The maximum temperature rise of 6.2 K was recorded at a depth of 35.5 m (Figure 5b), and the minimum temperature rise of 3.7 K was found at 74.5 m (Figure 5b). The smaller temperature increases and declining rise of the temperature at a depth of 74.5 m indicate a more significant convection in the gravelly sand sediments at this depth range.

The groundwater flow rate is estimated based on the MILS model and correlation parameters ($\Delta T(t_\infty)$, r/B, A) as given in Equation 11. As shown in Equation 14, further (merged) parameters need to be specified such as $\rho_w c_w$ of groundwater and $\lambda \rho c$ of the ground. The value of $\rho_w c_w$ without considering its change with temperature is assumed to be 4.2×10^6 J·m^{-3} K^{-1}. Based on Table 1 and empirical values of the grain density of the soil, the product $\lambda \rho c$ for different lithologies is approximated by the normal distribution $N(\mu, \sigma^2)$ considering the difference of the same lithology at different depths (Table S1 in Supporting Information S2).

The results are compared at this groundwater-influenced depth of 74.5 m with those for the assumed low-flow depth of 25.5 m. The solid lines in Figures 5b and 5c were obtained by fitting of Equation 11 using the Nelder-Mead simplex search method to the response data at different pre-set time stages (1–36, 3–36, 6–36 hr), as suggested in the previous theoretical analysis. At 25.5 m, the three fitted curves are close to each other, satisfactorily delineating the recorded thermal response data (Figure 5b). In comparison, the three fits at 74.5 m are not consistent. Apparently, there is not enough temperature change in the 6–36 hr phase data (Figure 5c), and the yellow line fitted to this phase deviates most from the measurements. The estimated flow rates at 74.5 m are 4.0×10^{-6}, 3.9×10^{-6}, and 4.1×10^{-6} m·s^{-1}, which correspond to pre-set different time stages (1–36, 3–36, 6–36). The result (4.1×10^{-6} m·s^{-1}) at the pre-set 6–36 hr time stage has a large difference to the ideal q value, which should be lower than 1×10^{-6} m·s^{-1}. Based on this preliminary analysis, it can be concluded that only the pre-set time stages of 1–36 and 3–36 hr may be helpful for evaluating the groundwater flow rate at the borehole.
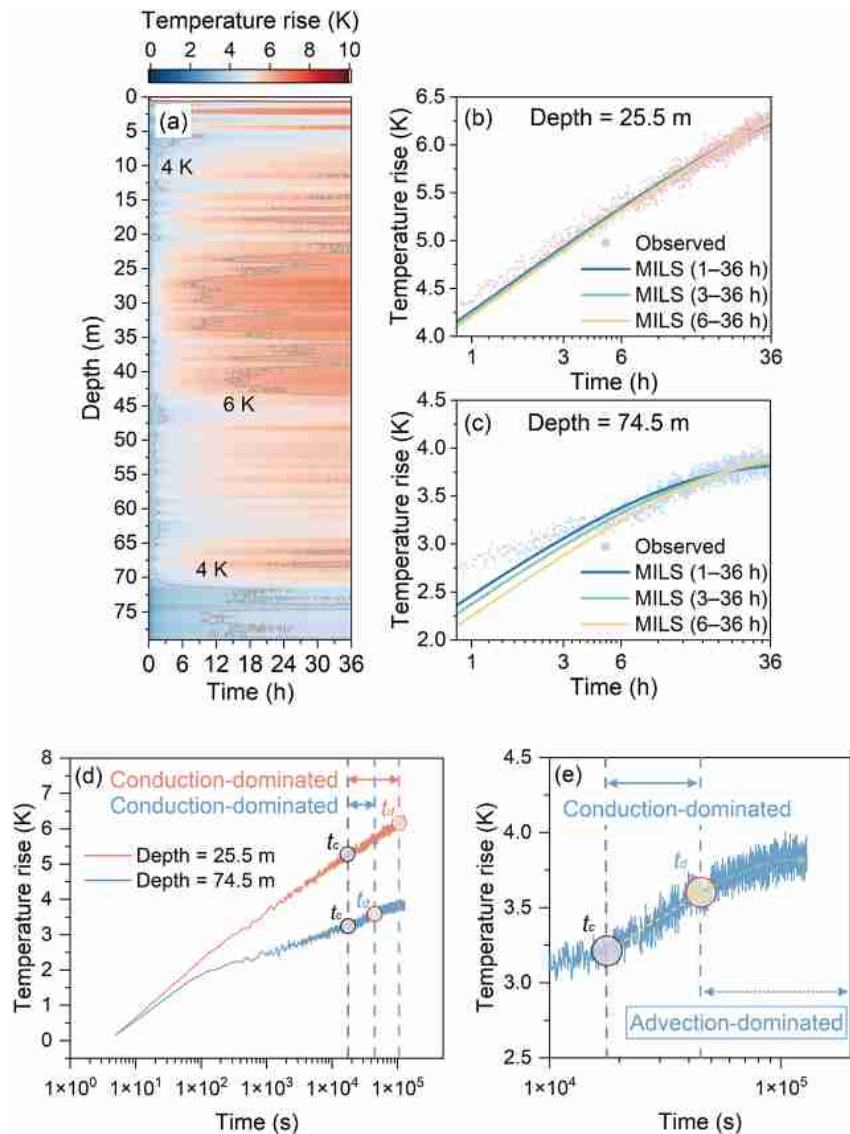
Figure 5. (a) Measured temperature response. In (b) and (c), the scattered points are the measured temperature response values, and the solid lines are the curves obtained by fitting the moving infinite line source (MILS) model for three different time periods. (d) Interpretation of the thermal response curve in depths of 25.5 and 74.5 m. (e) Zoomed view at thermal response curve in the depth of 74.5 m.

A comparison was made between Simon et al.'s method (Simon et al., 2021) and the procedure of this paper for the highlighted depths of 25.5 and 74.5 m. As t_c, according to Simon et al. (2021), represents the moment when the effect of the jacket can be ignored, this can be compared to the beginning of the S_g-phase in case of no groundwater flow ($t_c = 5.6$ hr). Following the steps recommended by Simon and Bour (2022), the suggested feature points were extracted, as shown in Figures 5d and 5e ($t_d = 4.4 \times 10^4$ s for 25.5 m, 1.1×10^5 s for 74.5 m). This means, as discussed in Section 3.1, that a smaller flow rate thus requires a longer TRT. Moreover, identifying feature points may become challenging when the temperature rise determined by the heating power is small.

The results of the mean groundwater rate estimation per depth are shown in Table S2 in Supporting Information S2. Both methods produce similar results in strata of different depths, supporting the feasibility of the new method. At 74.5 m, the groundwater flow rate estimated by the new method is 14% larger than by Simon et al. (2021)'s method. This may be attributed to an early selection of the time t_d, and the thermal conductivity calculated based on the conduction-dominant stage (2.5 W·m^{-1} K^{-1}) is slightly greater than the measured value (2.25 W·m^{-1} K^{-1}). Consequently, a portion of heat transfer by convection was attributed to conduction. The
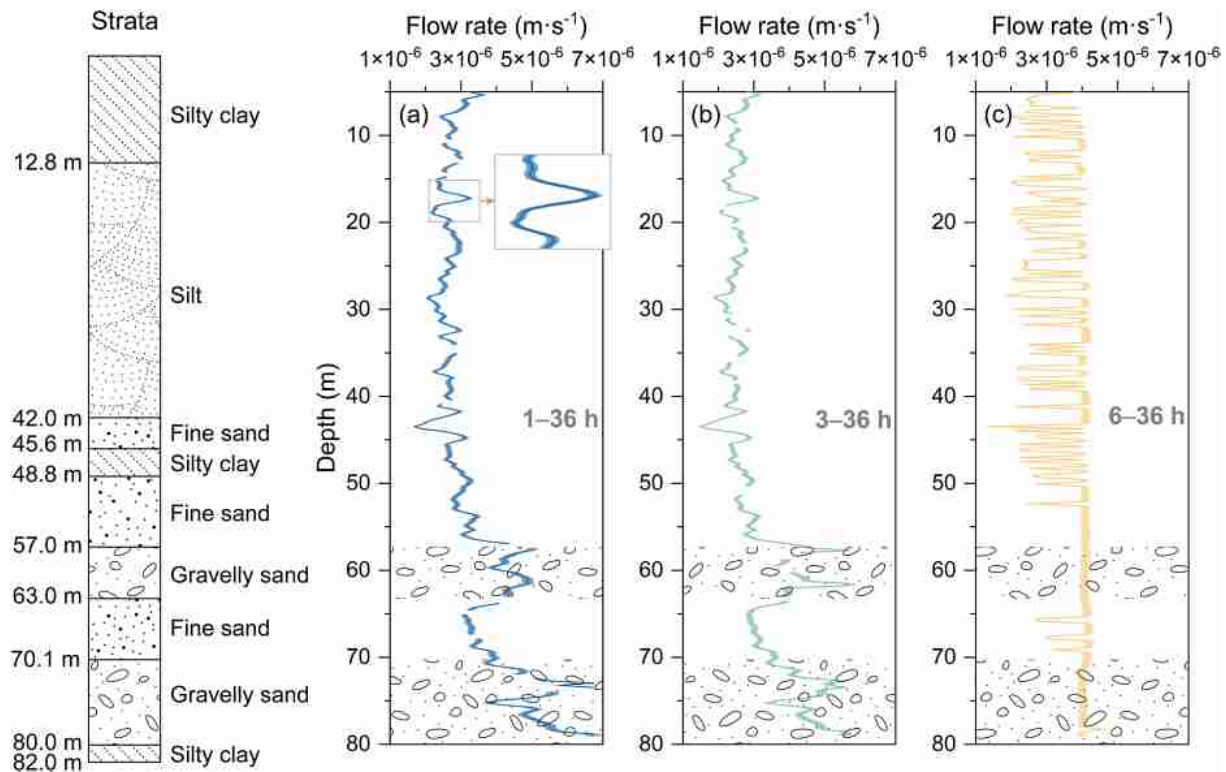
Figure 6. Groundwater flow rate and its 90% confidence interval estimated for different time stages: (a) 1–36 hr, (b) 3–36 hr, and (c) 6–36 hr for actively heated fiber-optic-based thermal response test (ATRT) field experiment.

estimation of groundwater flow rate is sensitive to the graphical identification of the time t_d and its error would be enhanced without considering the effect of the borehole. This demonstrates the potential of the new method to estimate the groundwater flow rate taking borehole effects into account also in case of grouted boreholes.

The estimated groundwater flow rates along the borehole are shown in Figure 6. A root derives an acceptable fit mean square error (RMSE) of less than 0.1 K, and the 90% confidence interval is calculated by the parameter values of the normal distribution in Table S1 in Supporting Information S2. The confidence interval has a mean width of 1.2×10^{-7} m·s^{-1}. This suggests that the groundwater flow rate estimation method is insensitive to $\lambda \rho c$ (Table S1 in Supporting Information S2), and thus a rough specification of $\lambda \rho c$ is sufficient. The calculated groundwater flow rates for three pre-set different time ranges (1–36, 3–36, 6–36 hr) are shown in Figures 6a–6c, respectively. The results obtained for 1–36 hr are generally consistent with those for 3–36 hr. The derived values of q range between 2×10^{-6} and 7×10^{-6} m·s^{-1}, which are compatible with the valid ranges given for this estimation period. Fitting the MILS to the period of 6–36 hr yields larger values than those in Figures 6a and 6b. However, the estimated groundwater flow rates between 2×10^{-6} and 5×10^{-6} m·s^{-1} are above the valid threshold of 1×10^{-6} m·s^{-1}. Thus, these values are not reliable. Figure 6c further reveals that the falsely estimated q varies significantly among the strata at varying depths, and obviously artifacts from the misfit minimization procedure cause this variation. These results illustrate those conditions considered above when discussing the numerical model application (Figure 4d), when curve fitting is compromised by scant temperature rise and temperature resolution. In contrast, a relatively short experimental time of 36 hr is needed for producing the results shown in Figure 6a, which are consistent with the estimated mean groundwater flow rate at the site.

The results obtained for 1–36 hr are used to describe the groundwater flow in the study area near the site of bank collapse. The average estimated groundwater flow rate by the new method in the study area (5–78 m) is 3.6×10^{-6} m·s^{-1}. The distribution of groundwater flow rate increased with depth and exhibited good agreement with the lithology of the strata (e.g., in gravelly sand, flow rates tend to be higher). The estimated q is relatively stable within 5–48.8 m with a mean value of 3.3×10^{-6} m·s^{-1}. These values agree with those values of 9×10^{-7} to 5×10^{-6} m·s^{-1} obtained independently by a pumping test in the top aquifer (12.8–45.6 m). As the pumping

test evaluates the whole aquifer, the difference could be found considering our groundwater observation results investigated different aquifer volumes. An even more pronounced velocity in the bottom aquifer was revealed. The average flow rates in the upper and lower gravelly sands of the bottom confined aquifer are 4.1×10^{-6} m·s^{-1} and 4.0×10^{-6} m·s^{-1}, respectively, with a peak of $q = 4.6 \times 10^{-6}$ m·s^{-1}.

4. Discussion

To illustrate the sensitivity and applicability of the novel method with several approximations, we discussed the ground thermal conductivity uncertainty and the effect of the grouted borehole on strata flow using synthetic data generated by the numerical models. Then, a flow chart further explains the estimation process and its portability.

4.1. Ground Thermal Conductivity Uncertainty

Obtaining accurate thermal conductivity of the ground can be challenging considering the in-situ condition and the differences between heat conduction and heat convection, either in the laboratory or in the field (He et al., 2018; Wagner, Bayer, et al., 2014; Wilke et al., 2020). Thus, inaccurate thermal conductivity may induce errors in estimating the groundwater flow rate. The propagation of thermal conductivity error on the groundwater flow rate estimation can be calculated based on Equation 14. The resulting error of estimated groundwater flow rate thus is derived by

$$\text{Error}_{\text{flow}} = 100 \cdot \left(\sqrt{1 \pm \frac{\lambda_{\text{error}}}{100 \cdot \lambda}} - 1 \right) \tag{16}$$

Accordingly, any uncertainty in the groundwater flow rate would only correspond to about half of the uncertainty of thermal conductivity. To further explore the effect of ground thermal conductivity uncertainty, we also used a Monte Carlo sampling of 10,000 points in the feasible parameter space, drawn from a uniform distribution of 1.3–2.3 W·m^{-1} K^{-1}. The error of the estimated flow velocity based on variable thermal conductivity could be found in Figure S2 in Supporting Information S1. As thermal properties of a homogeneous lithology are relatively constant (Ghanbarian & Daigle, 2016), a broad parameter value space (1.3–2.3 W·m^{-1} K^{-1}) would also represent the changes in lithology (like thin layers in the strata). The analysis shows that a thermal conductivity ($\lambda_{\text{error}} = -0.4$ W·m^{-1} K^{-1}) estimated with a considerable error of 22.2% would result in groundwater flow estimation inaccuracy of only 10.5%, and thermal conductivity ($\lambda_{\text{error}} = 0.4$ W·m^{-1} K^{-1}) with a −22.2% error would result in a value of −11.8%.

4.2. The Effect of the Grouted Borehole on Strata Flow

In the present method, the borehole penetrates layered ground built up by several strata. The flow rate in each stratum can be different, and the flow rate difference between grouted borehole and strata is neglected. If there is a significant difference in the hydraulic conductivity between the borehole and strata, this artificially introduces lateral heterogeneity. A numerical model was constructed to investigate the effect of the grouted borehole on strata flow. Three layers with different hydraulic conductivities (Layer 1 = 6×10^{-4} m·s^{-1}, Layer 2 = 6×10^{-5} m·s^{-1}, and Layer 3 = 5×10^{-5} m·s^{-1}) are modeled with a constant horizontal hydraulic gradient of 0.01 applied to the model boundaries in the x-axis. The borehole is in the center of the layers and has a radius of 0.065 m. Detailed model parameters are listed in Table S3 in Supporting Information S2. The model size is $1 \times 1 \times 15$ m. Groundwater flows are modeled with the Darcy's law interface in COMSOL Multiphysics® combined with "extremely fine triangular meshing law" based on model sizes (including 2,019,927 units with a 3.274×10^{-5} unit-area ratio in the 15 m^3 model).

The results obtained by the numerical simulation was shown in Figure S3 in Supporting Information S1. With increasing distance from the borehole center ($x = 0$ m), the borehole effect weakens, and the flow rate difference in the layers decreases. Following a distance of 0.2 m of ground in layers 1 and 3, a low error (close to the observation in the model boundary, $x = 0.5$ m) is found. Figure S3b in Supporting Information S1 depicts the radial distribution of the flow rate around the borehole. There is no clear evidence that the grouted borehole has a wide-ranging change in the flow in layers. With a flow change tolerance of 10%, a limited effect range ($x \leq 0.174$ m in layer 1, $x \leq 0.164$ m in layer 2) was recorded. des Tombe et al. (2019) claimed that the
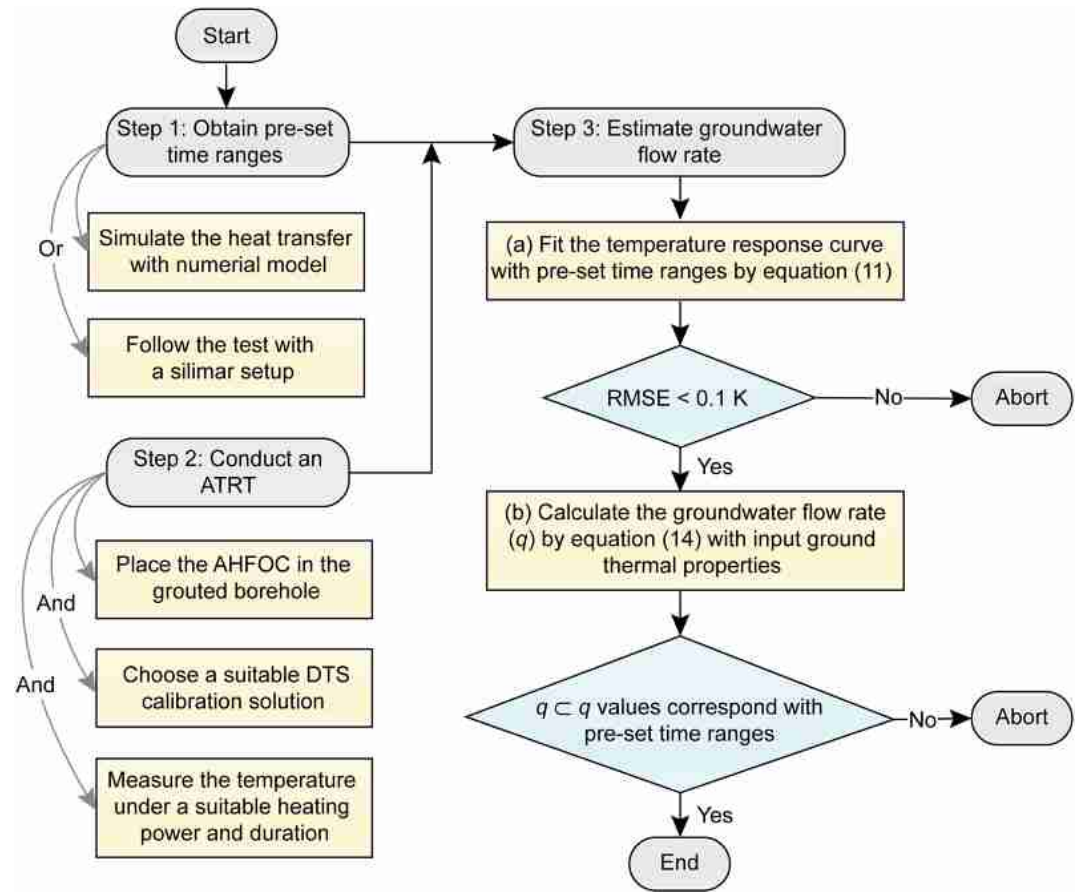
Figure 7. A flowchart for the estimation of groundwater rate in the grouted borehole.

measurement area (the area with the least 0.1 K temperature rise) was approximately 5.9 m^2 if the flow rate is 0.1 m/day and 8.3 m^2 if the flow rate is 0.5 m/day with a heat duration of 4.8 days. Taken together, these observations indicate that for the estimation procedure, the effect of a grouted borehole on strata flow is limited.

4.3. Applicability

The three major steps of the presented procedure are summarized in Figure 7: Step 1 is the numerical analysis (Figure 4) and MILS fitting procedure that is required to identify the valid time ranges for the corresponding values of q. This needs to be done for each different borehole configuration only once, and thus a separate, comprehensive analysis for typical borehole designs would simplify applicability in practice. Step 2 covers the application of the ATRT in the field, which includes placing the AHFOC in the borehole, DTS calibration, and subsequent heating. Step 3 is concerned with the groundwater flow rate estimation. This step consists of two parts. Here, Step 3a fits the temperature response curve (ATRT) according to Equation 7 within the previously defined pre-set time ranges, and an RMSE < 0.1 K ensures acceptable solutions. Step 3b calculates the flow rate by Equation 14 based on the known ground thermal properties. Only those results that pass the consistency check between estimated and suitable values of q (according to Step 1) are considered feasible.

To further explain the portability, it should be noted that the information about the pre-set time stages in this paper can be worked in other tests if researchers follow the AHFOC and borehole setup introduced in Section 2.3. Such a standardized strategy can significantly improve the efficiency of groundwater flow rate estimation. Additionally, the flow rate estimation quality is closely linked to if the ATRT was conducted as expected (like the consistency of the AHFOC location along the borehole and the choice of suitable temperature measurement resolution). And the judgment (RMSE <0.1 K) in Step 3a could also filter the coarse temperature solution data. Indeed, previous studies on TRTs indicate that the above effects of ATRT conduction could be minimized by prolonging the test

duration (Dalla Santa et al., 2022; B. Zhang et al., 2020; C. Zhang et al., 2014). Considering that the longer test duration means an additional cost, further research aims to fully understand the presented estimation method's sensitivity and could enhance its robustness for application to different sites.

5. Conclusions

This study proposes an in-situ method for estimating the groundwater flow rate in a grouted borehole. AHFOC is recommended as an effective tool for TRTs, and the estimation method of the groundwater flow rate is based on the MILS model. The estimation of groundwater flow rate in the ground can be achieved through three steps: (a) numerically analyze the effects of the borehole structure to determine the stage in which the thermal response curve satisfies the MILS model under different groundwater flow rate environments; (b) determine different time stages that cover the range of typical groundwater flow rates and calculate the corresponding groundwater flow rates by fitting the MILS model; (c) combine the findings of step (a) and compare the groundwater flow rate estimation results of different time stages to determine the true groundwater flow rate.

The proposed new method for estimating the flow rate was successfully applied to a grouted borehole near a bank collapse site, where groundwater flow was significant in two penetrated aquifer layers. The results indicate that the method is insensitive to the ground's thermal properties, and it can vertically resolve groundwater flow rates around the borehole. The average flow rate in the study area is estimated to be 3.6×10^{-6} m·s^{-1}. The flow rate $(3.4 \times 10^{-6}$ m·s$^{-1})$ in the top confined aquifer matches the groundwater flow measured by a pumping test in the study area. The average flow rate $(4.1 \times 10^{-6}$ m·s$^{-1})$ in the bottom confined aquifer indicates larger groundwater flow.

The new method ignores the influence of vertical heat transfer in different strata, and any in-well flow for estimating the groundwater flow rate. These factors may cause errors, yet a quantitative analysis of such influencing factors is rare. Recently, des Tombe et al. (2019) proposed that vertical heat transfer from different strata requires the TRT result combined with numerical models to estimate groundwater flow rates jointly. Discussing these influencing factors would be more difficult when considering transient heat transfer in composite media. In spite of this, the ATRT can be considered as an advanced method, which provides a refined estimation of the groundwater flow rate in the grouted borehole with a high resolution in depth.

Abbreviations

AHFOC	actively heated fiber-optic cable
ATRT	actively heated fiber-optics-based thermal response test
ILS	infinite line source
MILS	moving infinite line source
RMSE	root mean square error
TRT	thermal response test

Nomenclature

A	substitute for $r^2/4D$
B	substitute for $2D\rho c/q_w c_w$
$\mathbf{D}$	thermal dispersion tensor (m^2·s^{-1})
D	thermal diffusivity (m^2·s^{-1})
n	total porosity (%)
P	volumetric heat generation in the source term (W·m^{-3})
K_0	modified Bessel function of the second kind and order zero
p	specific heating power of the heating source (W·m^{-1})
$\mathbf{q}$	specific discharge vector (m·s^{-1})
q	specific discharge, Darcy flux (m·s^{-1})
r	radius of the heating source (m)
s	variable of integration in the Hantush well function
T	temperature (K)

t	time (s)
T_0	undisturbed temperature (K, °C)
t_c	time when the cable jacket effect becomes negligible in TRT (s)
t_d	time when groundwater flow begins affect the TRT (s)
t_i	time differentiating the conduction-dominant stage and convection-dominant stage in TRT (s)
t_s	time corresponding to steady state if $\Delta T = 0.99\Delta T(t_\infty)$ in TRT (s)
v	groundwater flow velocity (m·s^{-1})
v_{th}	thermal front velocity (m·s^{-1})
W	Hantush well function
x	x-axis location perpendicular to borehole in x-y plane (m)
y	y-axis location perpendicular to borehole in x-y plane (m)
ΔT	temperature rise (K)
$\Delta T(t_\infty)$	steady-state temperature rise (K)
λ	thermal conductivity (W·m^{-1} K^{-1})
ρc	volumetric heat capacity of bulk media (J·m^{-3} K^{-1})
$\rho_w c_w$	volumetric heat capacity of water (J·m^{-3} K^{-1})
$\rho_s c_s$	volumetric heat capacity of solid (J·m^{-3} K^{-1})

Data Availability Statement

Data and codes related to this manuscript can be downloaded from this repository: https://zenodo.org/record/6480800. The data consists of numerical data for analyzing the thermal response test and in situ measurements of an actively heated fiber-optics-based thermal response test in a grouted borehole. Codes for the pre-processing of the observational data and for estimating groundwater flow rates are written in MATLAB Live Script, version 2021b. Additional details are provided in Supporting Information S1 and S2.

References

Acuña, J., & Palm, B. (2013). Distributed thermal response tests on pipe-in-pipe borehole heat exchangers. *Applied Energy*, *109*, 312–320. https://doi.org/10.1016/j.apenergy.2013.01.024

Anderson, M. P. (2005). Heat as a ground water tracer. *Groundwater*, *43*(6), 951–968. https://doi.org/10.1111/j.1745-6584.2005.00052.x

Angelotti, A., Ly, F., & Zille, A. (2018). On the applicability of the moving line source theory to thermal response test under groundwater flow: Considerations from real case studies. *Geothermal Energy*, *6*(1), 1–17. https://doi.org/10.1186/s40517-018-0098-z

Bakker, M., Caljé, R., Schaars, F., van der Made, K. J., & de Haas, S. (2015). An active heat tracer experiment to determine groundwater velocities using fiber-optic cables installed with direct push equipment. *Water Resources Research*, *51*(4), 2760–2772. https://doi.org/10.1002/2014WR016632

Bayer, P., Rivera, J. A., Schweizer, D., Schärli, U., Blum, P., & Rybach, L. (2016). Extracting past atmospheric warming and urban heating effects from borehole temperature profiles. *Geothermics*, *64*, 289–299. https://doi.org/10.1016/j.geothermics.2016.06.011

Bense, V. F., Read, T., Bour, O., Le Borgne, T., Coleman, T., Krause, S., et al. (2016). Distributed temperature sensing as a downhole tool in hydrogeology. *Water Resources Research*, *52*(12), 9259–9273. https://doi.org/10.1002/2016WR018869

Bergman, T. L., Incropera, F. P., DeWitt, D. P., & Lavine, A. S. (2011). *Fundamentals of heat and mass transfer*. John Wiley & Sons.

Brunner, P., Therrien, R., Renard, P., Simmons, C. T., & Franssen, H. J. H. (2017). Advances in understanding river-groundwater interactions. *Reviews of Geophysics*, *55*(3), 818–854. https://doi.org/10.1002/2017RG000556

Cao, D., Shi, B., Zhu, H.-H., Wei, G., Bektursen, H., & Sun, M. (2019). A field study on the application of distributed temperature sensing technology in thermal response tests for borehole heat exchangers. *Bulletin of Engineering Geology and the Environment*, *78*(6), 3901–3915. https://doi.org/10.1007/s10064-018-1407-2

Dalla Santa, G., Pasquier, P., Schenato, L., & Galgaro, A. (2022). Repeated ETRTs in a complex stratified geological setting: High-resolution thermal conductivity identification by multiple linear regression. *Journal of Geotechnical and Geoenvironmental Engineering*, *148*(4), 04022007. https://doi.org/10.1061/(ASCE)GT.1943-5606.0002724

del Val, L., Carrera, J., Pool, M., Martínez, L., Casanovas, C., Bour, O., & Folch, A. (2021). Heat dissipation test with fiber-optic distributed temperature sensing to estimate groundwater flux. *Water Resources Research*, *57*(3), e2020WR027228. https://doi.org/10.1029/2020WR027228

des Tombe, B. F., Bakker, M., Smits, F., Schaars, F., & van der Made, K. J. (2019). Estimation of the variation in specific discharge over large depth using distributed temperature sensing (DTS) measurements of the heat pulse response. *Water Resources Research*, *55*(1), 811–826. https://doi.org/10.1029/2018WR024171

Diao, N., Li, Q., & Fang, Z. (2004). Heat transfer in ground heat exchangers with groundwater advection. *International Journal of Thermal Sciences*, *43*(12), 1203–1211. https://doi.org/10.1016/j.ijthermalsci.2004.04.009

Freifeld, B. M., Finsterle, S., Onstott, T. C., Toole, P., & Pratt, L. M. (2008). Ground surface temperature reconstructions: Using in situ estimates for thermal conductivity acquired with a fiber-optic distributed thermal perturbation sensor. *Geophysical Research Letters*, *35*(14), L14309. https://doi.org/10.1029/2008GL034762

Ghanbarian, B., & Daigle, H. (2016). Thermal conductivity in porous media: Percolation-based effective-medium approximation. *Water Resources Research*, *52*(1), 295–314. https://doi.org/10.1002/2015WR017236

Gu, X., Jiang, Y., Yang, G., Jin, Y., Mei, S., & Zhang, H. (2021). Stability analysis of dual structure bank slope under the condition of water level fluctuation: Take the bank of Zhinancun bank collapsed in Yangzhong city as an example. *East China Geology*(1), 76–84. https://doi.org/10.16788/j.hddz.32-1865/P.2021.01.009

Hakala, P., Vallin, S., Arola, T., & Martinkauppi, I. (2021). Novel use of the enhanced thermal response test in crystalline bedrock. *Renewable Energy*, *182*, 467–482. https://doi.org/10.1016/j.renene.2021.10.020

Hantush, M. S. (1956). Analysis of data from pumping tests in leaky aquifers. *Eos, Transactions American Geophysical Union*, *37*(6), 702–714. https://doi.org/10.1029/TR037i006p00702

He, H., Dyck, M. F., Horton, R., Ren, T., Bristow, K. L., Lv, J., & Si, B. (2018). Development and application of the heat pulse method for soil physical measurements. *Reviews of Geophysics*, *56*(4), 567–620. https://doi.org/10.1029/2017RG000584

Hermans, T., Goderniaux, P., Jougnot, D., Fleckenstein, J., Brunner, P., Nguyen, F., et al. (2022). Advancing measurements and representations of subsurface heterogeneity and dynamic processes: Towards 4D hydrogeology. *Hydrology and Earth System Sciences Discussions*, 1–55. https://doi.org/10.5194/hess-2022-95

Herrera-García, G., Ezquerro, P., Tomás, R., Béjar-Pizarro, M., López-Vinielles, J., Rossi, M., et al. (2021). Mapping the global threat of land subsidence. *Science*, *371*(6524), 34–36. https://doi.org/10.1126/science.abb8549

Hoffmann, R., Maréchal, J. C., Selles, A., Dassargues, A., & Goderniaux, P. (2021). Heat tracing in a fractured aquifer with injection of hot and cold water. *Groundwater*, *60*(2), 192–209. https://doi.org/10.1111/gwat.13138

Kavanaugh, S. P., & Rafferty, K. D. (2014). *Geothermal heating and cooling: Design of ground-source heat pump systems*. ASHRAE.

Klepikova, M. V., Roques, C., Loew, S., & Selker, J. (2018). Improved characterization of groundwater flow in heterogeneous aquifers using granular polyacrylamide (PAM) gel as temporary grout. *Water Resources Research*, *54*(2), 1410–1419. https://doi.org/10.1002/2017WR022259

Kurylyk, B. L., & Irvine, D. J. (2016). Analytical solution and computer program (FAST) to estimate fluid fluxes from subsurface temperature profiles. *Water Resources Research*, *52*(2), 725–733. https://doi.org/10.1002/2015WR017990

Liu, G., Knobbe, S., & Butler, J., Jr. (2013). Resolving centimeter-scale flows in aquifers and their hydrostratigraphic controls. *Geophysical Research Letters*, *40*(6), 1098–1103. https://doi.org/10.1002/grl.50282

Liu, H., Gu, K., Zhang, B., Wei, Z., Luo, Q., Shi, B., & Su, J. (2021). The influence of simplified line source on ATRT's calculation of soil thermal conductivity—Numerical simulation research. *East China Geology*, *42*(2), 157–166. https://doi.org/10.16788/j.hddz.32-1865/P.2021.02.004

Liu, Q., Hu, R., Hu, L., Xing, Y., Qiu, P., Yang, H., et al. (2022). Investigation of hydraulic properties in fractured aquifers using cross-well travel-time based thermal tracer tomography: Numerical and field experiments. *Journal of Hydrology*, *609*, 127751. https://doi.org/10.1016/j.jhydrol.2022.127751

Molina-Giraldo, N., Bayer, P., & Blum, P. (2011). Evaluating the influence of thermal dispersion on temperature plumes from geothermal systems using analytical solutions. *International Journal of Thermal Sciences*, *50*(7), 1223–1231. https://doi.org/10.1016/j.ijthermalsci.2011.02.004

Molina-Giraldo, N., Bayer, P., Blum, P., & Cirpka, O. A. (2011). Propagation of seasonal temperature signals into an aquifer upon bank infiltration. *Groundwater*, *49*(4), 491–502. https://doi.org/10.1111/j.1745-6584.2010.00745.x

Molina-Giraldo, N., Blum, P., Zhu, K., Bayer, P., & Fang, Z. (2011). A moving finite line source model to simulate borehole heat exchangers with groundwater advection. *International Journal of Thermal Sciences*, *50*(12), 2506–2513. https://doi.org/10.1016/j.ijthermalsci.2011.06.012

Munn, J., Maldaner, C., Coleman, T., & Parker, B. (2020). Measuring fracture flow changes in a bedrock aquifer due to open hole and pumped conditions using active distributed temperature sensing. *Water Resources Research*, *56*(10), e2020WR027229. https://doi.org/10.1029/2020WR027229

Nield, D. A., & Bejan, A. (2006). *Convection in porous media*. Springer.

Pasquier, P. (2018). Interpretation of the first hours of a thermal response test using the time derivative of the temperature. *Applied Energy*, *213*, 56–75. https://doi.org/10.1016/j.apenergy.2018.01.022

Pouladi, B., Bour, O., Longuevergne, L., de La Bernardie, J., & Simon, N. (2021). Modelling borehole flows from distributed temperature sensing data to monitor groundwater dynamics in fractured media. *Journal of Hydrology*, *598*, 126450. https://doi.org/10.1016/j.jhydrol.2021.126450

Raymond, J., Lamarche, L., & Malo, M. (2015). Field demonstration of a first thermal response test with a low power source. *Applied Energy*, *147*, 30–39. https://doi.org/10.1016/j.apenergy.2015.01.117

Read, T., Bour, O., Selker, J., Bense, V., Le Borgne, T., Hochreutener, R., & Lavenant, N. (2014). Active-distributed temperature sensing to continuously quantify vertical flow in boreholes. *Water Resources Research*, *50*(5), 3706–3713. https://doi.org/10.1002/2014WR015273

Sarris, T. S., Close, M., & Abraham, P. (2018). Using solute and heat tracers for aquifer characterization in a strongly heterogeneous alluvial aquifer. *Journal of Hydrology*, *558*, 55–71. https://doi.org/10.1016/j.jhydrol.2018.01.032

Selker, F., & Selker, J. S. (2018). Investigating water movement within and near wells using active point heating and fiber optic distributed temperature sensing. *Sensors*, *18*(4), 1023. https://doi.org/10.3390/s18041023

Selker, J., van de Giesen, N., Westhoff, M., Luxemburg, W., & Parlange, M. B. (2006). Fiber optics opens window on stream dynamics. *Geophysical Research Letters*, *33*(24), L24401. https://doi.org/10.1029/2006GL027979

Simon, N., & Bour, O. (2022). An ADTS Toolbox for automatically interpreting active distributed temperature sensing measurements. *Groundwater*. https://doi.org/10.1111/gwat.13172

Simon, N., Bour, O., Faucheux, M., Lavenant, N., Le Lay, H., Fovet, O., et al. (2022). Combining passive and active distributed temperature sensing measurements to locate and quantify groundwater discharge variability into a headwater stream. *Hydrology and Earth System Sciences*, *26*(5), 1459–1479. https://doi.org/10.5194/hess-26-1459-2022

Simon, N., Bour, O., Lavenant, N., Porel, G., Nauleau, B., Pouladi, B., et al. (2021). Numerical and experimental validation of the applicability of active-DTS experiments to estimate thermal conductivity and groundwater flux in porous media. *Water Resources Research*, *57*(1), e2020WR028078. https://doi.org/10.1029/2020WR028078

Spitler, J. D., & Gehlin, S. E. (2015). Thermal response testing for ground source heat pump systems—An historical review. *Renewable and Sustainable Energy Reviews*, *50*, 1125–1137. https://doi.org/10.1016/j.rser.2015.05.061

Stauffer, F., Bayer, P., Blum, P., Giraldo, N. M., & Kinzelbach, W. (2019). *Thermal use of shallow groundwater*. CRC Press. https://doi.org/10.1201/b16239

Sutton, M. G., Nutter, D. W., & Couvillion, R. J. (2003). A ground resistance for vertical bore heat exchangers with groundwater flow. *Journal of Energy Resource Technology*, *125*(3), 183–189. https://doi.org/10.1115/1.1591203

Van de Ven, A., Koenigsdorff, R., & Bayer, P. (2021). Enhanced steady-state solution of the infinite moving line source model for the thermal design of grouted borehole heat exchangers with groundwater advection. *Geosciences*, *11*(10), 410. https://doi.org/10.3390/geosciences11100410

Verdoya, M., Pacetti, C., Chiozzi, P., & Invernizzi, C. (2018). Thermophysical parameters from laboratory measurements and in-situ tests in borehole heat exchangers. *Applied Thermal Engineering*, *144*, 711–720. https://doi.org/10.1016/j.applthermaleng.2018.08.039

Wagner, V., Bayer, P., Bisch, G., Kübert, M., & Blum, P. (2014a). Hydraulic characterization of aquifers by thermal response testing: Validation by large-scale tank and field experiments. *Water Resources Research*, *50*(1), 71–85. https://doi.org/10.1002/2013WR013939

Wagner, V., Bayer, P., Kübert, M., & Blum, P. (2012). Numerical sensitivity study of thermal response tests. *Renewable Energy*, *41*, 245–253. https://doi.org/10.1016/j.renene.2011.11.001

Wagner, V., Blum, P., Kübert, M., & Bayer, P. (2013). Analytical approach to groundwater-influenced thermal response tests of grouted borehole heat exchangers. *Geothermics*, *46*, 22–31. https://doi.org/10.1016/j.geothermics.2012.10.005

Wagner, V., Li, T., Bayer, P., Leven, C., Dietrich, P., & Blum, P. (2014b). Thermal tracer testing in a sedimentary aquifer: Field experiment (Lauswiesen, Germany) and numerical simulation. *Hydrogeology Journal*, *22*(1), 175–187. https://doi.org/10.1007/s10040-013-1059-z

Wilke, S., Menberg, K., Steger, H., & Blum, P. (2020). Advanced thermal response tests: A review. *Renewable and Sustainable Energy Reviews*, *119*, 109575. https://doi.org/10.1016/j.rser.2019.109575

Xue, Y., Xie, C., & Li, Q. (1990). Aquifer thermal energy storage: A numerical simulation of field experiments in China. *Water Resources Research*, *26*(10), 2365–2375. https://doi.org/10.1029/WR026i010p02365

Ye, S., Xue, Y., & Xie, C. (2004). Application of the multiscale finite element method to flow in heterogeneous porous media. *Water Resources Research*, *40*(9). https://doi.org/10.1029/2003WR002914

Yeh, T.-C., Khaleel, R., & Carroll, K. C. (2015). *Flow through heterogeneous geologic media*. Cambridge University Press. https://doi.org/10.1017/CBO9781139879323

Yu, J., Wei, N., Jiang, R., Lao, J., Ma, X., Zhang, Z., & Zhao, L. (2013). Types, characteristics and genetic mechanisms of bank collapse in the Zhenjiang-Taizhou reach of Yangtze River. *East China Geology*, *34*(2), 127–132. https://doi.org/10.3969/j.issn.1671-4814.2013.02.009

Zhang, B., Gu, K., Shi, B., Liu, C., Bayer, P., Wei, G., et al. (2020). Actively heated fiber optics based thermal response test: A field demonstration. *Renewable and Sustainable Energy Reviews*, *134*, 110336. https://doi.org/10.1016/j.rser.2020.110336

Zhang, C., Guo, Z., Liu, Y., Cong, X., & Peng, D. (2014). A review on thermal response test of ground-coupled heat pump systems. *Renewable and Sustainable Energy Reviews*, *40*, 851–867. https://doi.org/10.1016/j.rser.2014.08.018

Zhang, C. C., Shi, B., Zhu, H. H., Wang, B. J., & Wei, G. Q. (2020). Toward distributed fiber-optic sensing of subsurface deformation: A theoretical quantification of ground-borehole-cable interaction. *Journal of Geophysical Research: Solid Earth*, *125*(3), e2019JB018878. https://doi.org/10.1029/2019JB018878

Zhao, P., Li, X., Zhang, Y., Liu, K., & Lu, M. (2020). Stratified thermal response test measurement and analysis. *Energy and Buildings*, *215*, 109865. https://doi.org/10.1016/j.enbuild.2020.109865

Zhu, M., Zuoqin, Z., & Rongyao, J. (2018). Study on evolution trend of Taipingzhou channel in Yangzhong reach of the Yangtze River. *Jiangsu Water Resources*, *07*, 58–61. https://doi.org/10.16310/j.cnki.jssl.2018.07.012